J. Fluid Mech. (1993), *vol.* 248, *pp.* 129–151

Non-steady peristaltic transport in finite-length tubes

By MEIJING LI AND JAMES G. BRASSEUR

Department of Mechanical Engineering, Pennsylvania State University, University Park PA 16802, USA

(Received 9 October 1991 and in revised form 8 September 1992)

The classical lubrication-theory model of steady peristaltic transport of periodic sinusoidal waves in infinite-length tubes (Shapiro *et al.* 1969) is generalized to arbitrary wave shape and wavenumber in tubes of finite length. Whereas the classical model is steady in a frame of reference moving with the peristaltic waves, peristaltic transport in a finite-length tube is inherently non-steady. It may be shown, however, that pumping performance is independent of tube length if there exists an integral number of peristaltic waves in the tube. Three particularly interesting characteristics of non-steady peristalsis are described: (i) fluctuations in pressure and shear stress arise due to a non-integral number of waves in the finite-length tube; (ii) retrograde motion of fluid particles during peristaltic transport (reflux) has inherently different behaviour with single peristaltic waves as compared to multiple 'train waves', and (iii) finite tube length, the number of peristaltic waves and the degree of tube occlusion affect global pumping performance. We find that, whereas significant increases in pressure and shear stress result from the tube-to-wave length ratio being non-integral, global pumping performance is only slightly degraded by the existence of a non-integral number of waves in the tube during peristaltic transport. Furthermore, the extent of retrograde motion of fluid particles is much greater with single waves than with train waves. These results suggest that in the design and analysis of peristaltic pumps attention should be paid to the unsteady effects of finite tube length and to the differences between single and multiple peristaltic waves.

1. Introduction

Peristaltic pumping is the process of fluid transport arising from the progression of contraction waves along a distensible tube. In the human body peristalsis is the primary physiological mechanism used to move fluids from one place to another. Examples include the passage of urine from the kidneys to the bladder, the movement of chyme in the gastro-intestinal tract and the transport of a food bolus through the oesophagus. Peristalsis is the mechanism used in blood pumps and is commercially applied in the transport of materials which must be kept uncontaminated or which are corrosive and must be separated from the pump machinery.

The earliest models of peristaltic pumping assumed trains of periodic sinusoidal waves in infinitely long two-dimensional channels or axisymmetric tubes (Shapiro 1967; Fung & Yih 1968; Yih & Fung 1969; Shapiro, Jaffrin & Weinberg 1969). These models, which were applied primarily to characterize the basic fluid mechanics of the pumping process, fall into two classes: (i) the model developed by Fung & Yih which is restricted to small peristaltic wave amplitudes but has no restrictions on Reynolds

number; and (ii) the lubrication-theory model introduced by Shapiro *et al.* (1969) in which effects of fluid inertia and wall curvature are neglected but no restrictions are placed on wave amplitude (see the review paper by Jaffrin & Shapiro 1971). The lubrication-theory model is applicable globally in the limit of totally occluding peristaltic waves and is found to be a reasonably accurate approximation of global pumping characteristics at a small Reynolds number and wall curvature (Jaffrin 1973; Takabatake & Ayukawa 1982; Takabatake, Ayukawa & Mori 1988). The accuracy of the model has been confirmed experimentally by Latham (1966) and Weinberg, Eckstein & Shapiro (1971). For many biological systems, particularly for peristaltic transport through the oesophagus and small bowels, the fluid bolus is sufficiently viscous, and the peristaltic wavelength sufficiently long, to justify application of the lubrication-theory approximations.

The classical lubrication-theory model of peristaltic pumping has been extended by several authors to include effects of non-Newtonian fluids (Shukla *et al.* 1980; Shukla & Gupta 1982; Bohme & Friedrich 1983) and different cross-sectional shapes (Jaffrin & Meginniss 1971; Rath 1982). Studies of pressure within the ureter showed that the pressure signature within the fluid bolus near the contraction region is very sensitive to wall shape (Lykoudis & Roos 1970; Brasseur & Dodds 1991). Roos & Lykoudis (1971) studied the effects of an inserted catheter on the fluid mechanics of urethral peristaltic transport. To explore the effects of a mucous layer in the gastrointestinal tracts, Brasseur, Corrsin & Lu (1987) studied the effects of a peripheral layer of different viscosity adjacent to the tube wall during peristalsis. Numerical calculations (Tong & Vawter 1972; Brown & Hung 1977; Stavitsky, Macagno & Christensen 1981; Takabatake & Ayukawa 1982; Takabatake *et al.* 1988; Dusey, Brasseur & Li 1990) which have appeared in the literature mainly as extensions to the two-dimensional wall models, have been used primarily to explore basic fluid mechanics issues rather than to describe a particular physiological flow.

Much of the fundamental physics underlying peristaltic pumping has been explored using the models mentioned above. In particular, these models have quantified the global performance of peristaltic pumps and have uncovered the phenomena of fluid particle 'reflux' and 'trapping'. However, these studies universally assumed an infinite train of peristaltic waves of prescribed shape travelling along an infinitely long tube. The more realistic, but inherently unsteady, model of a finite-length peristaltic pump has never been explored. In particular, the characteristics of single-wave peristaltic transport, as exists in oesophageal peristalsis, for example, or the effects of a non-integral number of waves in a finite tube, as is typical in commercial pumps, have not been studied. These issues underlie the present study.

We generalize the classical lubrication-theory model of peristaltic transport to allow for arbitrary wave shape, arbitrary wavenumber and finite tube length, with two primary motivations in mind. The motivations of the current paper are basic fluid mechanical issues of the non-steady effects associated with finite tube lengths and the inherent difference between single and multiple wave transport. A second motivation, to be reported in another paper, is the application of the generalized model to the simulation and biological study of oesophageal bolus transport.

Most of the previous studies of peristaltic pumping have concentrated on pumping performance as measured through global variables. In the current discussions we focus on two important local variables, pressure and shear stress, in addition to volume flow rate and pressure difference between the end of the tube. The mathematical details of the model will be given in the next section. Section 3

discusses effects associated with a non-integral number of peristaltic waves in a finite-length tube. In particular, we concentrate on the effects of fluctuating pressure and shear stress, and degradation of pumping performance associated with non-integral numbers of peristaltic waves. In §4, differences between single- and train-wave peristaltic transport are explored. We address, specifically, basic differences in particle reflux associated with single *vs.* multiple waves, and net reflux in comparison with the classical infinite-tube models. Conclusions follow in §5.

2. The mathematical model

In modelling the general case of non-periodic peristaltic transport in finite-length tubes, one must consider the inherently non-steady nature of the flow. Application of the lubrication-theory approximations to the non-steady problem requires that the flow dynamics be dominated by a single peristalsis-driven timescale and highly disparate single axial *vs.* radial lengthscales, and that the flow be driven by frictional forces.

Consider the schematic illustrations of peristaltic transport in figure 1. Figure 1 (*a*) illustrates a single wave moving along a finite tube, whereas figure 1 (*b*) illustrates the continual production of multiple 'train waves'. We apply the lubrication-theory approximations to peristaltic transport driven by arbitrarily shaped deformations of the tube wall with pressure boundary conditions at the tube ends. Axisymmetric flow in a tube of circular cross-section is assumed with a single-phase Newtonian incompressible fluid of uniform viscosity μ. The characteristic velocity of the peristaltic wave is c, the wavelength of the peristaltic wave is λ, the tube is of length L and the minimum tube radius, or 'tube occlusion', is ϵ. The shape of the tube wall is given by $H(x,t)$. In the model, each material point on the wall moves only radially with velocity $\partial H(x,t)/\partial t$. (Longitudinal motions may be shown to be a second-order effect under conditions of small wall curvature (e.g. Taylor 1951)). Uniform pressures, p_0 and p_L, are applied to the inlet and the outlet of the tube ($x = 0, L$), respectively. The fluid volume within a single peristaltic wave, the 'bolus', is V_B. The problem is formulated in the 'laboratory frame', whereby the observer is fixed relative to the tube ends as the peristaltic waves move past.

Mathematically, the cases of single *vs.* multiple peristaltic waves (figure 1*a* and 1*b*) are handled in the same way. To apply lubrication theory to the general non-steady problem, the dominant axial scale λ is assumed to be large relative to the dominant radial scale, a, where a is taken to be the average radius of the bolus, $a \equiv (V_B/\pi\lambda)^{\frac{1}{2}}$. In peristaltically driven flows the appropriate timescale is the wave period, λ/c. In the general non-steady case, λ, a and c are average values over time. If the temporal variations are such that a, λ, L, λ/c, and c are the only dominant space, time, and velocity scales, then the appropriate normalizations for viscous-dominated flows are

$$x = \frac{\hat{x}}{\lambda}, \quad r = \frac{\hat{r}}{a}, \quad t = \frac{c\hat{t}}{\lambda}, \quad U = \frac{\hat{U}}{c}, \quad V = \frac{\hat{V}}{kc}, \quad p = \frac{\hat{p}a^2}{\mu c\lambda},$$

where $\hat{U}$, and $\hat{V}$ are the axial and radial velocity components, and k is a wavenumber given by $k = a/\lambda$. Correspondingly, the only appropriate Reynolds number is given by

$$Re = (\rho ca/\mu)\, k.$$

To simplify the problem, we introduce the lubrication theory approximations of infinitesimally small wall curvature ($k \to 0$) and Reynolds number ($Re \to 0$). The approximations assume that inertial effects are negligible and that the dominant

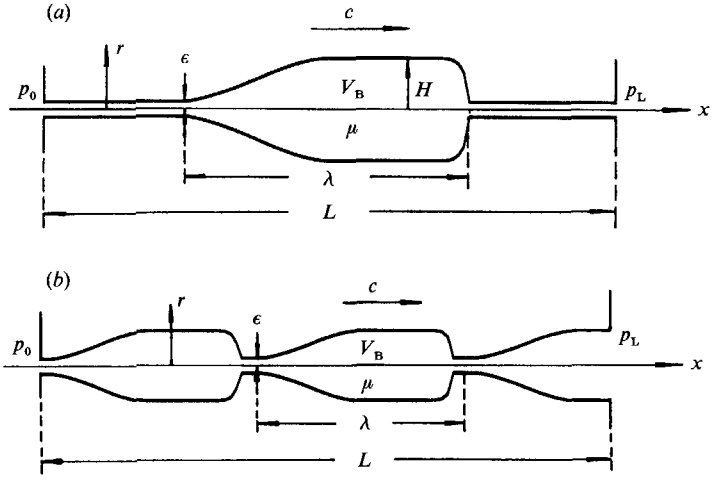

FIGURE 1. Sketch of peristaltic transport: (*a*) illustrates a single contraction wave, whereas (*b*) illustrates the continual production of 'train waves'. In both cases, the fluid bolus is transported from left to right against a pressure difference $p_L - p_0$ by peristaltic contraction waves along the tube. The contraction wave speed, wavelength, tube length and tube occlusion are defined respectively as c, λ, L and ϵ. The fluid viscosity and the fluid volume within one wavelength (the bolus) are μ and V_B. A non-integral number of peristaltic waves in the tube ($L/\lambda \neq$ integer) is illustrated in (*b*).

axial scale is much larger than the dominant radial scale. In this limit, pressure is uniform on each cross-section and the governing equations and boundary conditions become

$$\frac{\partial p}{\partial x} = \frac{1}{r}\frac{\partial}{\partial r}\left(r\frac{\partial U}{\partial r}\right); \quad \frac{1}{r}\frac{\partial (rV)}{\partial r} + \frac{\partial U}{\partial x} = 0, \tag{1}$$

$$U|_{r=H} = 0, \quad V|_{r=H} = \frac{\partial H}{\partial t}; \quad \left.\frac{\partial U}{\partial r}\right|_{r=0} = 0, \quad V|_{r=0} = 0, \tag{2}$$

$$p|_{x=0} = p_0, \quad p|_{x=L} = p_L, \tag{3}$$

where $H = \hat{H}/a$ and $L = \hat{L}/\lambda$. The lubrication-theory approximations lead to a local Poiseuille flow at every cross-section which communicates with its neighbouring sections through continuity. Uniform pressure must be specified at the two ends of the tube. The limits $k \to 0$ and $Re \to 0$ provide reasonably good global approximations even when the curvature and the Reynolds number are finite but small (Jaffrin 1973; Takabatake & Ayukawa 1982; Takabatake *et al.* 1988).

The velocity field is obtained from (1):

$$U = \frac{1}{4}\frac{\partial p}{\partial x}(r^2 - H^2), \tag{4}$$

$$V = \frac{r}{4}\left[H\frac{\partial H}{\partial x}\frac{\partial p}{\partial x} - \frac{\partial^2 p}{\partial x^2}(\tfrac{1}{4}r^2 - \tfrac{1}{2}H^2)\right]. \tag{5}$$

Evaluating (5) at the wall produces a relationship between the motion of the tube wall and the axial pressure gradient $\partial p/\partial x$:

$$\frac{H^3}{16}\frac{\partial^2 p}{\partial x^2} + \frac{H^2}{4}\frac{\partial H}{\partial x}\frac{\partial p}{\partial x} = \frac{\partial H}{\partial t}. \tag{6}$$

Integrating once yields

$$\frac{\partial p}{\partial x} = \frac{1}{H^4(x,t)}\left(G_0(t) + 16\int_0^x H(s,t)\frac{\partial H(s,t)}{\partial t}\,\mathrm{d}s\right), \tag{7}$$

where $G_0(t)$, at most, depends on time. Integrating a second time yields a relationship between intraluminal pressure, wall geometry and wall velocity:

$$p(x,t) = p_0(t) + \int_0^x \frac{\partial p}{\partial x}(s,t)\,\mathrm{d}s. \tag{8}$$

$G_0(t)$ is determined by evaluating (8) at $x = L$ where $p = p_L$:

$$G_0(t) = \frac{\Delta p(t) - 16\int_0^L H^{-4}(s_1,t)\left(\int_0^{s_1} H(s_2,t)\frac{\partial H(s_2,t)}{\partial t}\,\mathrm{d}s_2\right)\mathrm{d}s_1}{\int_0^L H^{-4}(s,t)\,\mathrm{d}s}. \tag{9}$$

Here $\Delta p = p_L(t) - p_0(t) = \Delta p(t)$ in general. Note from (7) and (8) that, as a consequence of the lubrication-theory approximations, temporal variations in pressure arise only through temporal variations at the inflow/outflow boundaries and temporal variations in wall velocity. Furthermore, pressure responds instantaneously to wall motions and the boundary conditions.

Equations (4) and (5) for the velocity field, and (7)–(9) for the pressure and pressure gradient fields effectively complete the solution. In carrying out the numerical integrations of (7)–(9), some care must be taken. This is especially true for the integration $\int H\,(\partial H/\partial t)\,\mathrm{d}x$ where inaccurate evaluation can lead to large error in the pressure.

The trajectories of fluid particles are obtained by carefully integrating particle velocity in time using second-order quadrature. Local wall shear stress is given by

$$\tau_w(x,t) = \left.\frac{\partial U}{\partial r}\right|_{r=H} = \frac{1}{2}\frac{\partial p}{\partial x}H. \tag{10}$$

How one non-dimensionalizes volume flow rate, $Q(x,t)$, depends on the characteristics of the peristaltic pump. For a periodic train of peristaltic waves moving at a constant speed, it is useful to normalize the dimensional flow rate

$$\hat{Q}(\hat{x},\hat{t}) = 2\pi\int_0^{\hat{H}} \hat{U}\hat{r}\,\mathrm{d}\hat{r}$$

with the flow rate of a completely occluded pump averaged over one wave period, $\pi a^2\lambda/\hat{T}_\lambda$, where $\hat{T}_\lambda = \lambda/c$. For transport by a single peristaltic wave, on the other hand, we normalize $\hat{Q}(\hat{x},\hat{t})$ with the flow rate of a completely occluded pump averaged over the period during which the wave moves from the inlet through the outlet of the tube, $\pi a^2\lambda/\hat{T}_L$, where $\hat{T}_L = L/c$. Consequently, the non-dimensional flow rate may be written

$$Q(x,t) = c_Q\,\hat{Q}/(\pi c a^2),$$

where $c_Q = 1$ for train waves and $c_Q = L/\lambda$ for single-wave transport. $Q(x,t)$ is therefore given by

$$Q(x,t) = 2c_Q\int_0^H Ur\,\mathrm{d}r = -\frac{c_Q}{8}\frac{\partial p}{\partial x}H^4. \tag{11}$$

Pumping performance is characterized by the relationship between a time-averaged volume flow rate,

$$\bar{Q} = \frac{1}{T}\int_{t_0}^{t_0+T} Q(x,t)\,\mathrm{d}t,$$

and the pressure difference between the ends of the tube, Δp, where Δp is fixed in time (see Shapiro *et al.* 1969). With periodic-train-wave peristaltic pumps, the average flow rate $\bar{Q}$ is defined over a single wave period, $T = 1$. In this case, the average volume flow rate $\bar{Q}$ is independent of t_0 and x. With single-wave transport, however, the average is taken over the time that the wave travels the length of the tube, $T = L/\lambda$, and $\bar{Q}(x)$ depends on the position in the tube there the average is taken. The relationship between $\bar{Q}$ and Δp is found by substituting (7) and (9) into (11):

$$\bar{Q} = \bar{Q}_0(1-\Delta p/\Delta p_0), \tag{12}$$

where

$$\bar{Q}_0 = \frac{2c_Q}{T}\int_0^T \frac{\displaystyle\int_0^L H^{-4}(s_1,t)\left(\int_x^{s_1} H(s_2,t)\frac{\partial H(s_2,t)}{\partial t}\,\mathrm{d}s_2\right)\mathrm{d}s_1}{\displaystyle\int_0^L H^{-4}(s,t)\,\mathrm{d}s}\,\mathrm{d}t, \tag{13}$$

$$\Delta p_0 = \frac{8\bar{Q}_0}{c_Q}\left[\frac{1}{T}\int_0^T \frac{\mathrm{d}t}{\displaystyle\int_0^L H^{-4}\,\mathrm{d}x}\right]^{-1}. \tag{14}$$

$\bar{Q}_0$ is the 'maximal' flow rate at x, the averaged flow rate when $\Delta p = 0$. Δp_0 is the pressure difference required to maintain zero net flow rate at x (i.e. when $\bar{Q}(x) = 0$).

Equations (4)–(14) provide the variables of interest in the current study. It may be shown that these equations reduce to the forms given by Shapiro *et al.* (1969) when the tube contains an integral number of periodic waves, that is when $H(x,t) = H(x-t)$. In what follows we analyse characteristics of finite-tube peristaltic pumps and single-wave peristaltic transport through parametric variation in L/λ, non-dimensional pressure difference Δp, peristaltic wave shape, and the degree of tube occlusion defined by the non-dimensional minimum radius in the tube ϵ/a. In comparing peristaltic pumps with different ϵ/a, Δp, or L/λ, the volume within one peristaltic wave is held fixed.

3. Effects of non-integral numbers of train waves

The studies of Shapiro and his colleagues concentrated on the global performance of peristaltic pumps with periodic sinusoidal waves in infinitely long tubes. Shapiro *et al.* found that particles near the walls of the pump tend to travel against the direction of the peristaltic wave when the pump operates against a positive pressure head.

In this section we consider the effect of finite tube length on transport characteristics. As pointed out in the previous section, pumping performance will only differ from the infinite-tube model if a non-integral number of peristaltic waves exists within the tube. In addition, we consider the effects of finite tube length on local variables, specifically pressure and wall shear stress. Pressure, in particular, is an important mechanical variable in biological systems such as the oesophagus, where intraluminal manometry is a common diagnostic tool used to evaluate the

contractile characteristics of the circular muscle within the oesophageal wall. The characteristics of pressure and shear stress fluctuations are also of interest in the design of commercial pumps where material fatigue is a concern.

3.1. *Pressure and shear stress fluctuations*

Consider first an integral number of train waves propagating with constant speed through a tube of finite length with fixed equal pressure at the inlet and the outlet of the tube. In this section the shape of the tube is sinusoidal, described by

$$H(x,t) = \epsilon/a + 0.5A\,[1-\cos 2\pi(x-t)]. \tag{15}$$

L/λ is varied by altering the length of the tube relative to the wave. When ϵ/a is varied, the wave amplitude A is adjusted to keep the volume of fluid within one wave fixed. Figure 2 shows pressure variations at six specially chosen times during one wave period with two waves existing in the tube ($L/\lambda = 2$). In this figure, the solid lines are the pressure distributions along the tube and the dashed lines are the corresponding wall shapes. In the calculation the initial location of the peristaltic wave is chosen with the point of minimum radius positioned at the inlet of the tube. All variables are non-dimensional as described in §2.1.

Note from figure 2 that within each peristaltic wave there exist two peaks in the pressure distribution with a gradual pressure ramp in between. The transition from a large negative peak to a large positive peak takes place at the point of minimum radius (the point of maximal occlusion) within the contraction zones. To the right of this point the tube wall is moving radially inward ($\partial H/\partial t < 0$), creating a large gradient in pressure there. In the oesophagus, for example, this radially inward motion of the tube wall is produced by the contraction of circular muscles within the oesophageal wall. To the left of the point of maximal occlusion the tube wall is moving radially outward leading to a corresponding drop in pressure there (there is no physiological counterpart to this outward motion†).

Note that at the point of maximal occlusion the axial pressure gradient is positive and the local instantaneous flow is to the left. In all other regions of the tube, however, the axially pressure gradient is negative and the local instantaneous flow is to the right – in the direction of the peristaltic wave. When averaged over one wave period, the net effect is transport in the direction of peristaltic wave motion.

It is typical for highly occluded peristaltic pumps (in figure 2, $\epsilon/a = 0.018$) to have large pressure gradients near the points of maximal occlusion, but a relatively small pressure gradient within the main body of the peristaltic wave. Less highly occluded pumps show a similar pressure distribution but with lower peak pressures, lower pressure gradients in the contraction zones, and a larger pressure gradient within the main body of the peristaltic wave relative to that within the contraction zone.

As shown in figure 2, the existence of fixed pressure conditions at the ends of the finite-tube peristaltic pump leads to a global fluctuation in the pressure with a period equal to that of a single peristaltic wave. The pressure distribution oscillates as a whole to maintain fixed pressure at the tube ends. The oscillation is particularly rapid when a contraction zone passes into and out of the tube due to the large local

† It is of interest to note that nearly all analyses of peristaltic transport, including the current one, are based on a model in which the shape of the peristaltic wave is assumed. Physiologically, peristaltic contractions arise from active tensile forces originating within the tube wall. Not all peristaltic wave shapes are compatible with physiologically realizable contractile forces. The commonly assumed sin-wave shape, for example, is associated with active compression at the proximal end of the wave, but active extension at the distal end of the wave; active extension can not occur in the physiological system. This issue will be discussed in detail elsewhere.

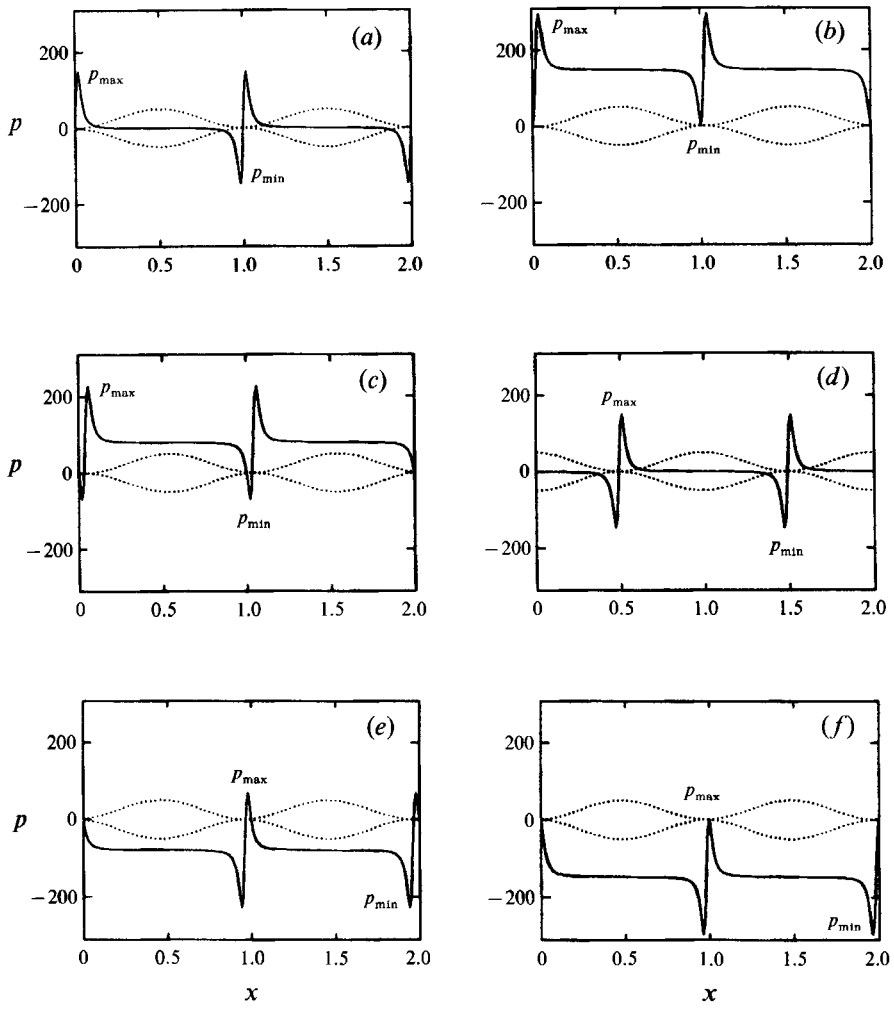

FIGURE 2. Pressure distributions along the tube at six time instants in one wave period with two waves in the tube ($L/\lambda = 2$): (*a*) $t = 0$; (*b*) 0.02; (*c*) 0.04; (*d*) 0.49; (*e*) 0.96; (*f*) 0.98. The solid lines are pressure distributions along the tube, and the dashed lines are the corresponding sinusoidal wall shapes. The maximum and minimum pressures along the tube at each time instant are marked with p_{max} and p_{min}, respectively. In response to the tube occlusion point moving into or out of the tube, the pressure distribution curves shift up and down as a whole. In the calculation, $p_L = p_0 \equiv 0$, $\epsilon/a = 0.018$, $A = 1.609$.

pressure variations in the region. Like the infinite-tube model, however, the relative difference in amplitude between the maximum pressure and minimum pressure, $\Phi \equiv p_{max} - p_{min}$, is invariant with time.

Shown in figure 3 is the time-varying pressure distribution for a non-integral number of peristaltic waves in the tube where all variables are the same as in figure 2 except for L/λ. Note that the spatial and temporal pressure distributions in these two cases are very different. In both cases fixed pressures at the tube ends force the pressure within a wave to oscillate as a unit, and the most rapid pressure variations take place as the contraction zone moves into or out of the tube ends. When an integral number of waves occupies the tube the peristaltic waves enter and leave the tube ends simultaneously, so the pressure waveform oscillates as a whole with a

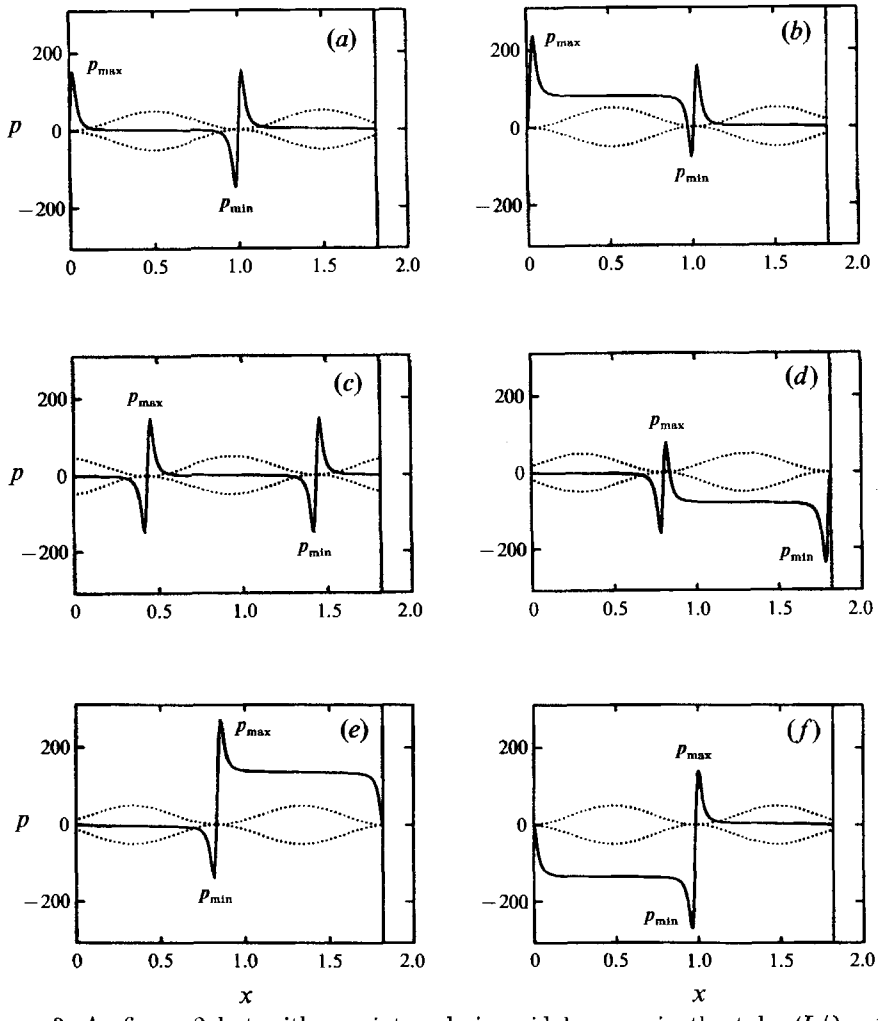

FIGURE 3. As figure 2 but with non-integral sinusoidal waves in the tube ($L/\lambda = 1.82$), and (*a*) $t = 0$; (*b*) 0.02; (*c*) 0.44; (*d*) 0.80; (*e*) 0.84; (*f*) 0.98. When the point of maximal tube occlusion moves into or out of the tube, the pressure waveforms oscillate rapidly.

period equal to the period of a single wave. With a non-integral number of waves, the wave entering the tube is out of phase with the wave exiting the tube, leading to a shift in the waveforms between the two waves and rather dramatic oscillations in Φ. The most rapid oscillations in Φ occur when a contraction zone passes through the inlet, or the exit, of the tube.

The most obvious difference between figures 2 and 3 is the variations of Φ with time. Φ fluctuates with time only when L/λ is non-integral, as can be seen in figure 4 for the two cases of figures 2 and 3, and for four additional values of L/λ ($L/\lambda = 1.0, 1.18, 1.82$ in figure 4*a* and $L/\lambda = 2.00, 2.18, 2.82$ in figure 4*b*). In all cases the only parameter varied is L/λ. The fluctuations in Φ are periodic with a period equal to the period of a single peristaltic wave. In the figure, solid curves are for cases where the fractional values of L/λ are greater than 0.5 and the dash-dot curves are for fractional values of L/λ are less than 0.5. Φ is constant and independent of L/λ when L/λ is an integer. When L/λ is not integral, on the other hand, Φ fluctuates with time above the value with an integral numbers of waves.

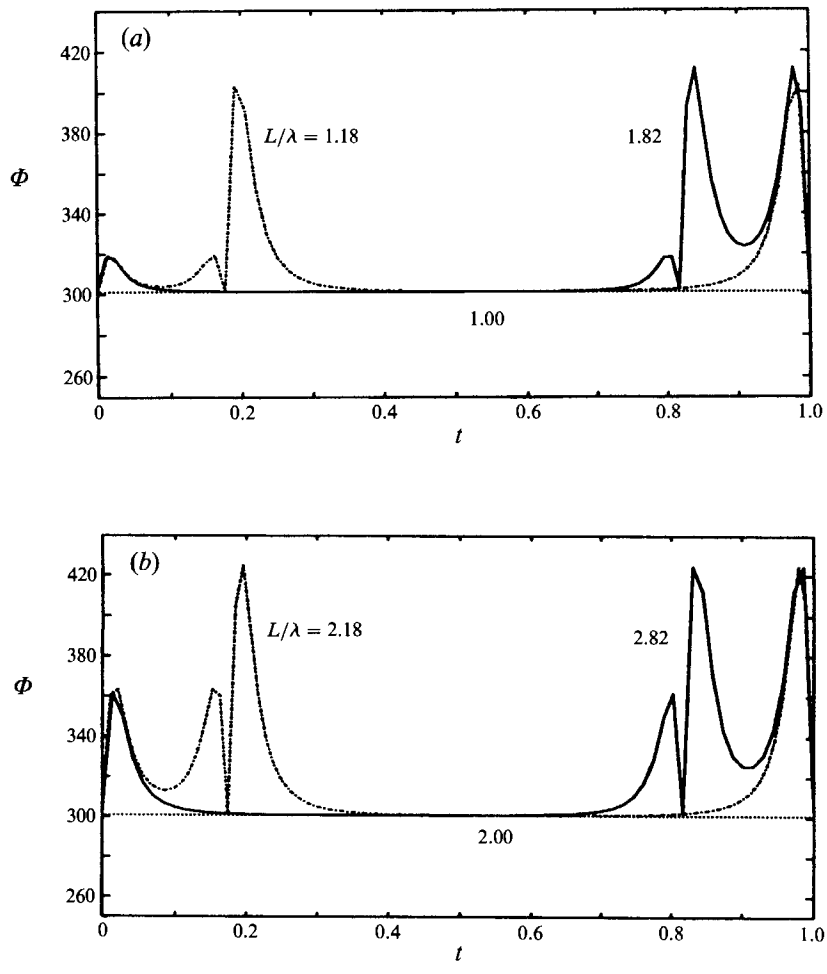

FIGURE 4. Temporal variations in pressure amplitude $\Phi \equiv p_{\max} - p_{\min}$ for different L/λ. The solid lines and dash-dot lines are for cases where the fractional values of L/λ are 0.82 and 0.18, respectively. Dotted lines are for integral tube-to-wave length. Note that Φ is time independent when L/λ is an integer. In all calculations, $p_L = p_0$, $\epsilon/a = 0.018$, $A = 1.609$.

Note that the fluctuation in Φ when L/λ is non-integral always occurs with two larger and two smaller peaks. When the fractional part of L/λ is greater than 0.5 the two smaller peaks surround the two larger peaks; the opposite is true when the fractional part of L/λ is less than 0.5 (the pattern repeats after $t = 1$). The demarcation time separating the two small peaks from the two large peaks in Φ always occurs at the beginning/end of each cycle, and at a time t_c which is given by the fractional part of L/λ (e.g. when $L/\lambda = 1.18$ $t_c = 0.18$, whereas when $L/\lambda = 1.82$ $t_c = 0.82$). This is because the fractional part of L/λ is equivalent to the non-dimensional time required for a most highly occluded point to reach the exit of the tube.

Because the lubrication theory approximations lead to local Poiseuille flow, the local flow rate and the wall shear stress distribution are directly proportional to the local pressure gradient. Local pressure gradients in the finite-tube and infinite-tube models are equivalent when the tube is filled with an integral number of peristaltic waves. However, when L/λ is non-integral, local pressure gradients may vary

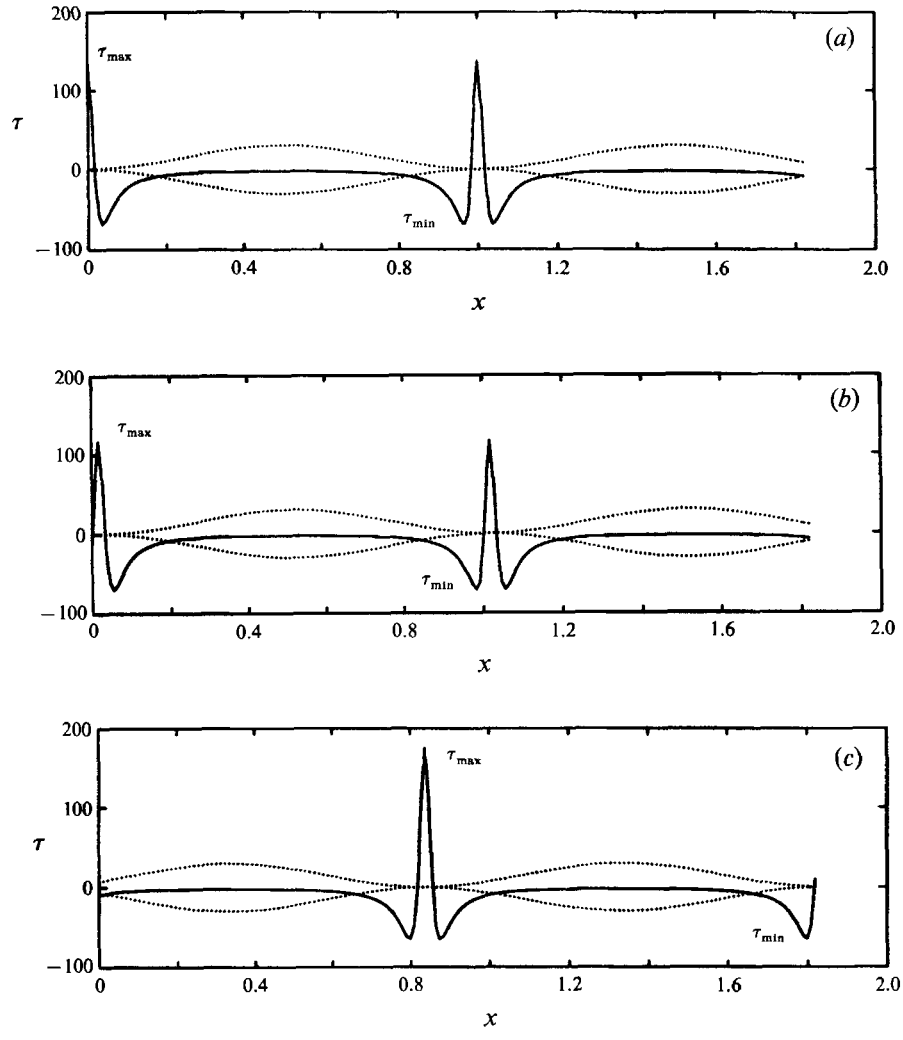

FIGURE 5. Wall shear stress distribution at three time instants: (*a*) $t = 0$; (*b*) 0.02; (*c*) 0.84. The solid lines are shear stress distributions, and the dotted lines are the corresponding wall shapes. The minimum and maximum wall shear stress at each time instant are marked with τ_{min} and τ_{max} which occurs at most highly occluded points. The shear stress distribution fluctuates as the peristaltic waves move into or out of the tube. In the calculations, $p_L = p_0$, $L/\lambda = 1.82$, $\epsilon/a = 0.018$, $A = 1.609$.

significantly over a peristaltic wave cycle, leading to fluctuations in wall shear stress not present in the integral wave case.

Figure 5 shows the shear stress distribution along the wall when $L/\lambda = 1.82$ at three different time instants. Comparing figure 5(*a*) with the local pressure distribution in figure 3(*a*), note that maximal positive wall shear stress τ_{max} occurs at the points of maximum pressure gradient, the most highly occluded points along the tube. Smaller peaks occur on either side of τ_{max}, when the local pressure gradient, and consequently the local flow, has changed direction. These negative peaks, labelled τ_{min} on figure 5, are not as large in magnitude as τ_{max}. Relative to the

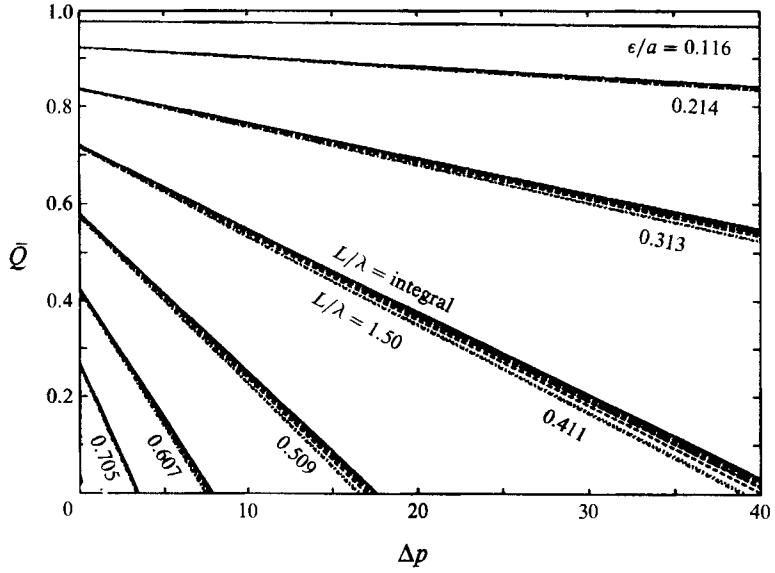

FIGURE 6. Pressure – volume flow rate characteristics of train wave peristaltic transport with different tube relative occlusions ϵ/a and different tube-to-wave lengths L/λ. The volume flow rate averaged over one wave period is plotted against pressure difference $\Delta p = p_L - p_0$ in groups for different ϵ/a, where L/λ is varied within each group from 1 to 4. In each group of fixed ϵ/a, the curves for integral L/λ overlap at the top of the group, whereas the curve for $L/\lambda = 1.5$ is always the lowest curve in the group. The effect of non-integral L/λ is to reduce the level of pumping for given pressure head with $L/\lambda = 1.5$ having greatest effect.

occluded zone which is a region of high shear stress, the central portion of a peristaltic wave is a region of relatively low shear stress.

Note from figures 3(*a*) and 3(*b*) that the local pressure gradient at the most highly occluded point decreases slightly between $t = 0$ and 0.02. Consequently, the maximal shear stress also decreases, as shown in figures 5(*a*) and 5(*b*). Similarly, the local pressure gradient reaches a maximum at the most highly occluded points at $t = 0.84$ (figure 3*e*) and $t = 0.98$ (figure 3*f*). At these times the local shear stress in these regions exceeds the maximum shear stress in the infinite-tube model (compare figures 5*c* and 5*a*).

3.2. *Peristaltic pumping performance*

In the analysis of peristaltic transport as a mechanical pump, pumping performance is measured as the average pumping flow rate for given pressure head against which the pump operates. The relationship between the pressure difference $\Delta p = p_L - p_0$ and the flow rate averaged over one wave period, $\bar{Q}$, is linear in the infinite-tube lubrication-theory model (Shapiro *et al.* 1969), but non-linear when a Newtonian peripheral layer exists adjacent to the tube wall (Brasseur *et al.* 1987). In the finite-tube homogeneous lubrication-theory model, the relationship between Δp and $\bar{Q}$ was shown to be linear in (12)–(14). When an integral number of waves exists in the tube, the pumping performance is that of the infinite-tube model. Of interest here is the effect of non-integral L/λ on pumping performance.

In the infinite-tube model $\bar{Q}$ is invariant with the axial position where the time average is carried out. Equations (12)–(14) show that in the finite-tube model the average volume flow rate $\bar{Q}$ is, in general, dependent on axial position x. However, if the peristaltic waves are periodic in x ($H(x,t) = H(x-t)$) the average volume flow

rate $\bar{Q}$ may be shown to be independent of x regardless of L/λ. This latter case is shown in figure 6, where Δp is plotted against $\bar{Q}$ for periodic train waves travelling along a tube of finite length. Within each group of curves ϵ/a is fixed and L/λ is varied from $L/\lambda = 1$ to $L/\lambda = 4$. Consistent with the usual definition of a mechanical pump, we consider only positive pressure heads ($\Delta p > 0$). Although the effect of non-integral L/λ is to reduce the level of pumping for given pressure head relative to integral L/λ (or the infinite-tube model), the effect is, in general, not very large.

4. Comparisons of single peristaltic waves with train waves

In the human body, propagating contraction waves often transport single boluses of physiological fluid from one place to another. We explore here the basic fluid dynamics of single-wave peristaltic transport in tubes of finite length in comparison with transport via train waves. In particular, we analyse fluid particle reflux in single bolus transport in comparison with train waves and quantify the net loss of fluid through the inlet of the tube as a single bolus traverses the tube. We find that significantly greater fluid particle reflux occurs with single-wave peristaltic transport than train waves.

4.1. *Difference in pressure and flow characteristics*

Before discussing the differences in reflux and pumping characteristics between single- and train-wave peristaltic transport, it is helpful to compare the spatial and temporal pressure variations in each case. This comparison is given in figure 7 where the spatial variations in pressure are plotted at fixed times for single bolus transport (*a–c*) and train-wave transport with a non-integral number of waves in the tube (*d–f*). In both cases $\Delta p = 0$, the wave shapes are sinusoidal, and all other conditions are the same. The solid lines give the pressure distributions along the tube and the dashed lines show the corresponding wall shapes.

In the single-wave case (*a–c*), an extended adverse pressure gradient is created by the peristaltic wave from the inlet of the tube to the tail and the outlet of the tube to the head of the peristaltic wave. These extended regions of adverse pressure gradient, where the flow is opposite to that of the peristaltic wave, do not exist in the train-wave case. Consequently, during its transit to the outlet of the tube a single peristaltic wave is followed by an ever-increasing region of retrograde flow. A region of retrograde flow exists at the outlet to the tube until the head of the peristaltic wave arrives at the outlet.

Until the peristaltic wave passes through the outlet, the single-wave pump acts to transport fluid in the opposite direction to the motion of the peristaltic wave. However, as the bolus passes through the outlet of the tube, it carries fluid along with it. Ultimately, net transport is in the direction of the peristaltic wave. This dual transport characteristic of single-wave pumps is shown clearly in figure 8 where the local flow rates at the outlet $Q(L,t)$ and the inlet $Q(0,t)$, as well as their corresponding running time averages

$$\bar{Q}_{\text{outlet}}(t) \equiv \frac{1}{t}\int_0^t Q(L,t')\,\mathrm{d}t', \quad \bar{Q}_{\text{inlet}}(t) \equiv \frac{1}{t}\int_0^t Q(0,t')\,\mathrm{d}t',$$

are plotted against time during the period that the peristaltic wave travels from the inlet through the outlet. Note that the local flow rate at the outlet is retrograde to the bolus motion until the bolus passes through the outlet. Net forward transport results from the expulsion of the transported bolus fluid from the tube. Interestingly,

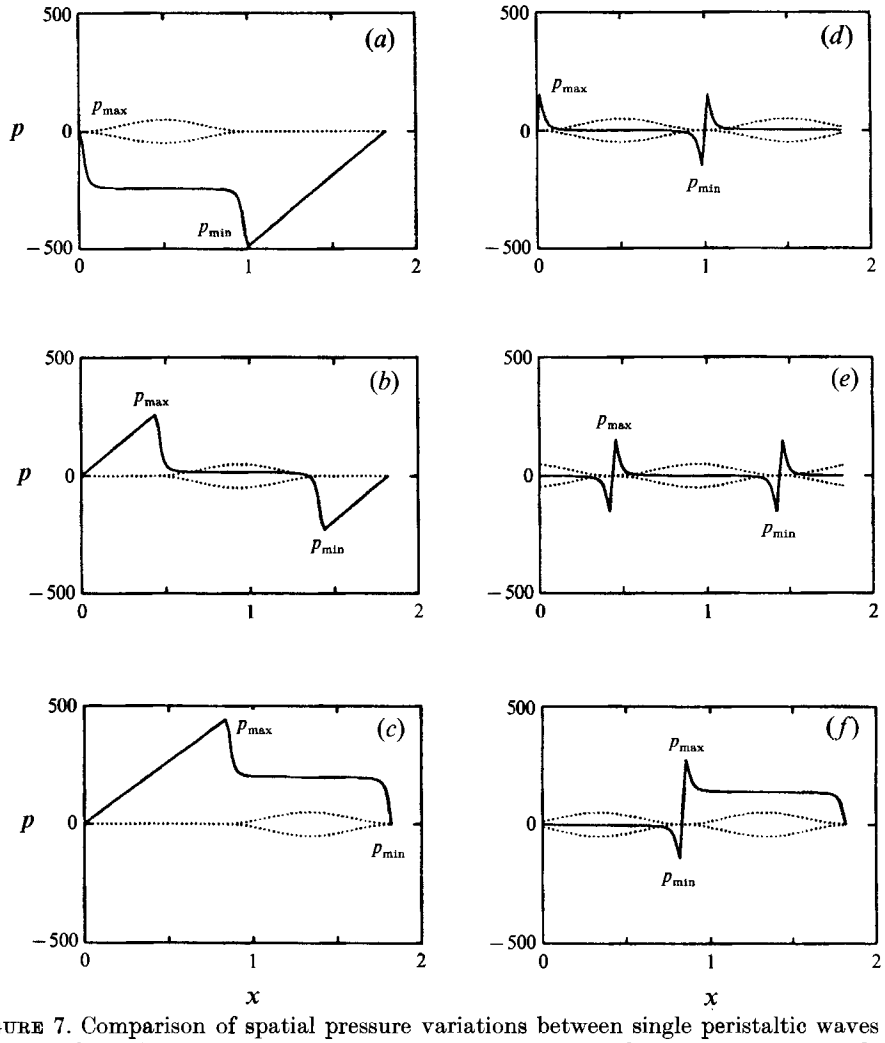

FIGURE 7. Comparison of spatial pressure variations between single peristaltic waves and train waves at three time instants over one wave period: (*a–c*) single wave transport, and (*d–f*) train wave transport; (*a*, *d*) $t = 0$; (*b*, *e*) 0.44; (*c*, *f*) 0.84. Solid lines are pressure distributions along the wall. The dashed lines show the corresponding wall shapes. The maximal and minimal pressures along the wall at each time instant are marked with p_{max} and p_{min}. In the calculation, $p_L = p_0 \equiv 0$, $L/\lambda = 1.82$, $\epsilon/a = 0.018$, and $A = 1.609$.

fluid continually leaves the tube inlet during single-bolus transport. This is not the case within train waves.

4.2. *Particle trajectory and reflux*

'Reflux' here refers to the presence of fluid particles that move, on average, in a direction opposite to that of the peristaltic wave†. The phenomenon was first elucidated by Shapiro *et al.* (1969) where it was found, in the infinite-tube model, that particle reflux occurs under conditions of partial occlusion and adverse net pressure

† 'Particle' reflux is distinguished from pressure-driven reflux which occurs, for example, when the sphincter guarding the lower oesophagus opens abnormally allowing gastric fluid to be forced into the lower oesophagus, and sometimes to the mouth.

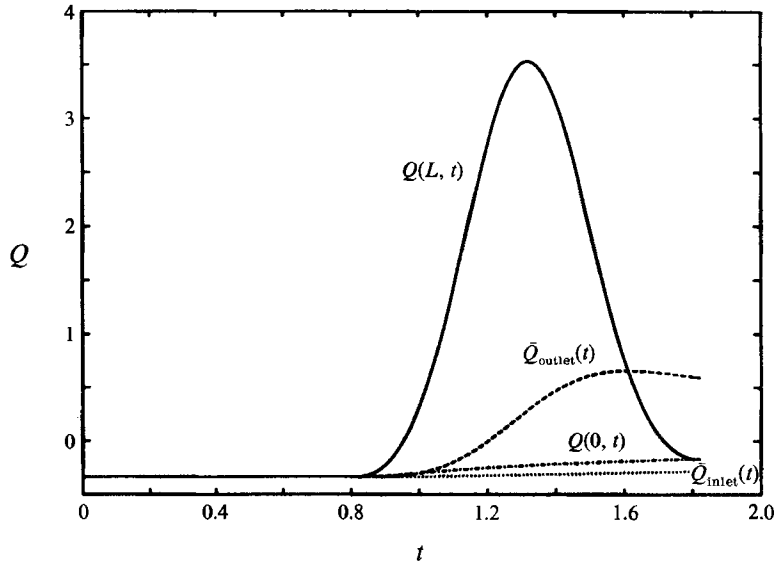

FIGURE 8. Volume flow rates at the tube inlet and outlet as a function of time. The local volume flow rates at the outlet and inlet, $A(L,t)$ and $Q(0,t)$ respectively, and their corresponding running averages, $\bar{Q}_{outlet}(t)$ and $\bar{Q}_{inlet}(t)$ are shown. In the calculation, $\Delta p = 47.15$, $L/\lambda = 1.82$, $\epsilon/a = 0.354$, and $A = 1.126$.

difference across one wavelength. Brasseur *et al.* (1987) found that the existence of a peripheral layer of fluid with different viscosity strongly influences the extent and degree of particle reflux. In these studies, however, only periodic train waves in infinitely long tubes were considered. In this section we study the effect of wave shape, non-integral numbers of peristaltic waves in the tube, and the differences between single- and train-wave peristaltic transport in the backward migration of fluid particles.

The basic geometry of single- and train-wave peristaltic transport was illustrated in figure 1. To study the effects of wave shape we compare the sinusoidal wave shape of (15) and figure 2 with the 'tear-drop' shape shown in figure 1, which is a more realistic model of bolus geometry in the oesophagus and other physiological systems. Particle trajectories of the following four cases are compared in figure 9 when an adverse pressure head is placed across the tube: (*a*) a single sinusoidal peristaltic wave, (*b*) train waves with a sinusoidal shape and (*c*) train waves with a tear-drop shape, where $L/\lambda = 5$ in all three cases; and (*d*) train waves with a sinusoidal shape but with a non-integral number of waves in the tube ($L/\lambda = 4.76$). All other conditions – fluid volume per wave, tube occlusion and length, wave speed, adverse pressure difference, fluid viscosity, and the initial positions of the fluid particles – are the same in the four calculations. The single-bolus case begins with the bolus centrally located in the tube. In all cases the trajectories of eight fluid particles are calculated, where the particles are initially placed on both sides of the peristaltic wave at the most highly occluded point, as shown in figure 9. The fluid particle trajectories are shown in figure 9 over three wave periods. Note that the radial scale has been highly stretched relative to the axial scale in these figures to better observe the radial motions of the fluid particles.

Figure 9(*b*) is the classical case of periodic sinusoidal wave contractions in an infinite tube with adverse pressure head. Note that, whereas most of the fluid

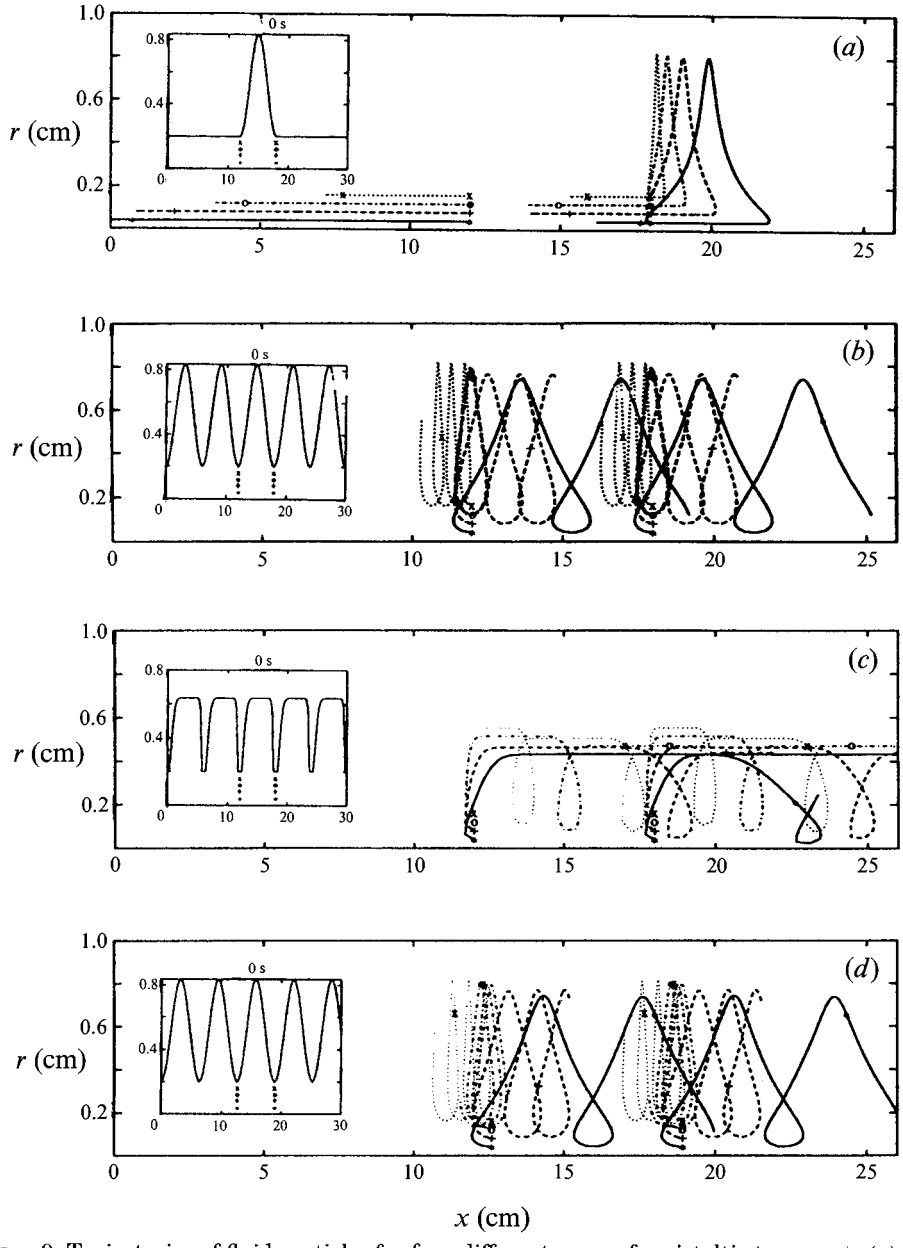

FIGURE 9. Trajectories of fluid particles for four different cases of peristaltic transport: (*a*) a single sinusoidal wave ($L/\lambda = 5$); (*b*) train of sinusoidal waves with integral $L/\lambda = 5$; (*c*) train of tear-drop-shaped waves with integral $L/\lambda = 5$; and (*d*) train of sinusoidal waves with non-integral $L/\lambda = 4.76$. In all calculations a non-dimensional adverse pressure difference of 18.85 was applied across the tube. Initially the fluid particles are located at $x = 12.0$ and 18.0 cm. $\epsilon/a = 0.354$ in all cases.

particles move, on average, in the direction of the peristaltic wave, the fluid particles nearest to the wall of the tube migrate in the opposite direction. Shapiro *et al.* (1969) found that the thickness of the region near the wall in which reflux occurs, and the relative flow rate in the reflux region, are strongly dependent on the degree of

occlusion and the magnitude of the adverse pressure difference across the ends of the pump. Comparison between figures 9(*b*) and 9(*c*) suggests that reflux is also strongly affected by the shape of the peristaltic wave. None of the fluid particles in figure 9(*c*) migrate in a retrograde direction. On the other hand, comparison of figure 9(*b*) with 9(*d*) indicates that only minimal differences exist between non-integral and integral numbers of peristaltic waves in the tube.

The most interesting observation from figure 9 is in the comparison of particle motions between the single peristaltic wave of figure 9(*a*), and the train waves of figures 9(*b*) and 9(*d*). Whereas in figures 9(*b*) and 9(*d*) only the fluid particles closest to the tube wall move in a direction opposite to the peristaltic wave, in the single bolus case all fluid particles initially in the occlusion zone ultimately move to positions to the left of their starting point during the time that the wave has travelled through the tube outlet. We find that, in general, significantly more fluid particle reflux occurs with single waves than with corresponding train-wave peristaltic transport during the same time period, and that the distance over which the refluxed particles migrate is much greater with single waves.

The observations above are further quantified in figure 10 where the trajectories of 451 particles, initially distributed over 41 uniformly spaced cross-sectional areas within the tube, are shown. In each of these cross-sections 11 particles are evenly spaced from the wall to the tube centre at the initial time. In the single-wave case, the peristaltic wave, initially located in the middle on the tube, passes the tube exit after three wave periods. The locations of each fluid particle relative to its starting point are recorded in all cases after three wave periods. Figure 10 shows the normalized distributions of relative particle motion for the four cases on figure 9.

It is immediately apparent from figure 10 that single-wave peristaltic transport (figure 10*a*) leads to substantially greater reflux than train-wave peristaltic transport (figure 10*b*). In fact, 77% of the fluid particles migrated to a position to the left of where they started ($x_s < 0$) with single-wave transport, whereas only 26% migrated to the left with periodic sinusoidal peristaltic waves over three wave periods. Consistent with the observations of figure 9, there is relatively little difference in the distributions of fluid particles between integral and non-integral numbers of peristaltic waves in the tube (compare figures 10*b* and 10*d*). On the other hand, tear-drop-shaped peristaltic waves (figure 10*c*) are considerably more effective in resisting particle reflux and enhancing forward motion of fluid particles than sinusoidal peristaltic waves (figure 10*b*). Only 2% of the 451 fluid particles moved in a retrograde direction with the tear-drop wave shape, as compared with 26% with sinusoidal peristaltic waves.

It is interesting to note one fundamental difference between cases with integral and non-integral numbers of peristaltic waves. We observed in discussing figure 9(*b*) that particles near the wall tend to move against the peristaltic wave, whereas particles near the centre of the tube move with the peristaltic wave. Between these two regions lie fluid particles which do not move in either direction, but move around closed loops. For example, the particles indicated with the symbol ○ in figure 9(*b*) are following such closed paths. No closed paths exist, however, when a non-integral number of waves occupies the tube. This is because the flow is inherently non-steady when L/λ is non-integral in all frames of reference, and periodic fluid motions do not occur. Consequently, all fluid particles migrate either with or against the peristaltic wave. However, the global differences between integral and non-integral numbers of train waves are relatively minor, as observed by comparing figures 10(*b*) and 10(*d*).

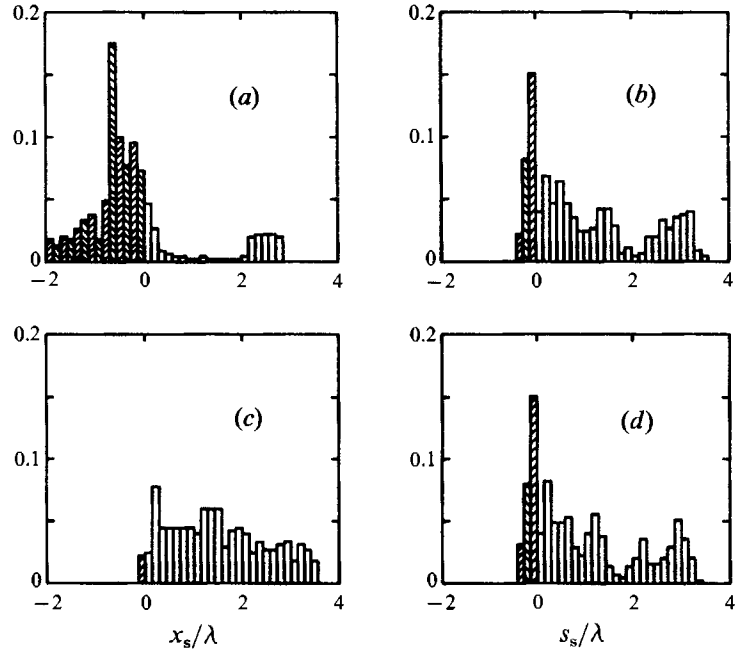

FIGURE 10. Distributions of the distance that fluid particles travel relative to their initial positions for the four cases of figure 9. The abscissa is the distance a particle has travelled, non-dimensionalized with the wavelength, after three wave periods. The distributions are normalized to unity. In all cases, a non-dimensional adverse pressure difference of 18.85 was applied across the tube ends, and the trajectories of 451 particles are calculated. At the initial time, the 451 particles are distributed at 41 uniformly spaced cross-sections, in each of which 11 particles are evenly placed from the wall to the centre of the tube. The hatched bars correspond to refluxed particles. Single-wave peristaltic transport leads to substantially greater reflux than train-wave peristaltic transport. $\epsilon/a = 0.354$ in all cases.

4.3. *Net loss of refluxed fluid from the tube inlet*

In the classical train-wave model, reflux can only occur with an adverse pressure difference across the tube. Consequently, net retrograde flow is caused by a pressure-driven component induced by the net increase in pressure along the peristaltic pump. We found in §4.1, however, that fluid continually leaves the tube inlet during single-wave peristaltic transport.

To quantify the net loss of fluid from the tube in single-bolus peristaltic transport, we average the volume flow rate at the inlet of the tube over the time that the peristaltic wave travels from the inlet to the outlet of the tube, as calculated from (12)–(14). In figure 11 the average flow rate leaving the inlet, $\bar{Q}_{\text{inlet}} < 0$, is plotted against a favourable pressure difference between the outlet and inlet of the tube. Groups of curves with fixed ϵ/a but different L/λ are given, showing that the influence of L/λ on flow rate is much weaker than the influence of ϵ/a. A number of interesting observations can be made from figure 11. Net fluid reflux takes place in the presence of a favourable pressure gradient. Indeed, a favourable pressure gradient is required to prevent reflux from the inlet to the tube. This circumstance is very different from the classical train-wave model where no reflux occurs unless an adverse pressure difference exists across the tube ends. Note from figure 11 that loss of fluid from the inlet of the pump cannot be prevented when $\Delta p = 0$.

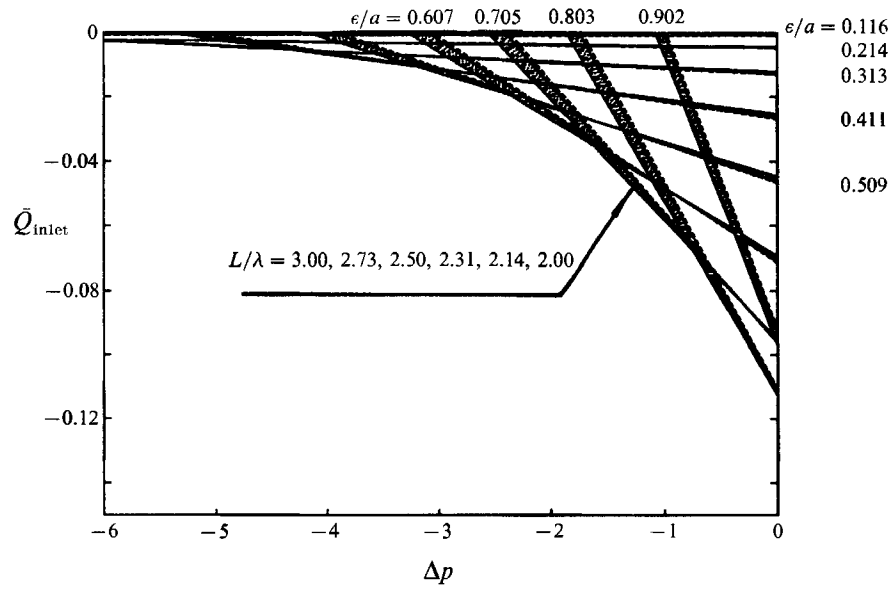

FIGURE 11. Pressure–volume flow rate characteristics of single-wave peristaltic transport with different relative tube occlusions ϵ/a and different tube-to-wave lengths L/λ. The average volume flow rate at the tube inlet $\bar{Q}_{\text{inlet}}$ is plotted against pressure difference $\Delta p = p_L - p_0$ in groups for different ϵ/a, where L/λ is varied within each group from 3 to 2 in the direction indicated by the arrow. A negative value of volume flow rate $\bar{Q}_{\text{inlet}}$ implies fluid reflux from the tube inlet.

Note that, as the level of occlusion increases (decreasing ϵ/a), the magnitude of the favourable pressure difference required to prevent reflux from occurring increases, although the amount of reflux at fixed Δp eventually becomes small for small enough ϵ/a. An interesting observation from figure 11 is that, for fixed negative (i.e. favourable) pressure difference Δp, the level of refluxed fluid does not diminish monotonically with decreasing ϵ/a. In figure 12 $\bar{Q}_{\text{inlet}}$ is plotted against ϵ/a for different fixed pressure difference Δp. Observe that, at fixed Δp, a critical occlusion exists at which the magnitude of refluxed fluid from the inlet to the tube is maximal. This critical occlusion shifts to smaller ϵ/a as the favourable pressure difference increases. Only as ϵ/a approaches 0 (complete occlusion) or 1 (no peristalsis) does reflux of fluid from the pump cease when $\Delta p = 0$.

4.4. *Pumping performance in single-wave peristaltic transport*

Figure 6 showed that, whereas non-integral numbers of train waves in the tube reducing pumping performance over integral numbers of waves, the effect is not great. The pumping performance of single-wave peristaltic transport is shown in figure 13, where Δp is plotted against $\bar{Q}_{\text{outlet}}$ in different groups of fixed ϵ/a, and L/λ is varied between 2 and 3 within each group. Note that $\bar{Q}_{\text{outlet}}$ and $\bar{Q}_{\text{inlet}}$ are averages over the period that the wave travels from the tube inlet to the tube outlet, and that during this period the fluid volume in the tube changes.

Pumping performance with single waves is qualitatively similar to that with train waves, as seen by comparing figure 13 with figure 6. With single waves, however, the 'maximal' flow rate $\bar{Q}_0$ is slightly less than with train waves, whereas the pressure difference required to maintain zero net flow rate is significantly greater than with train-wave peristaltic transport. Note also that pumping performance continuously

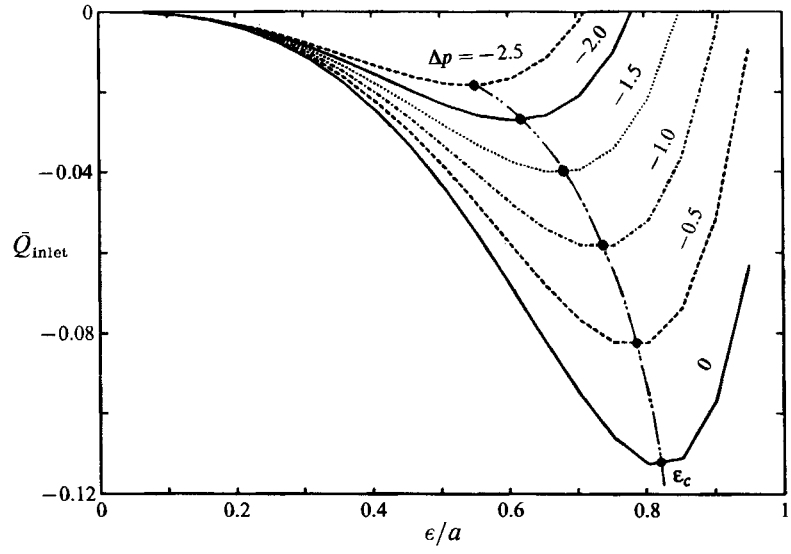

FIGURE 12. Average volume flow rate at the tube inlet $\bar{Q}_{\text{inlet}}$ as a function of tube occlusion ϵ/a for fixed favourable pressure difference Δp. A negative value of volume flow rate $\bar{Q}_{\text{inlet}}$ implies fluid reflux at the inlet. At fixed Δp a critical occlusion ϵ_c exists at which the amount of refluxed fluid from the inlet to the tube reaches a maximum. This critical occlusion shifts to smaller ϵ/a as the favourable pressure difference increases.

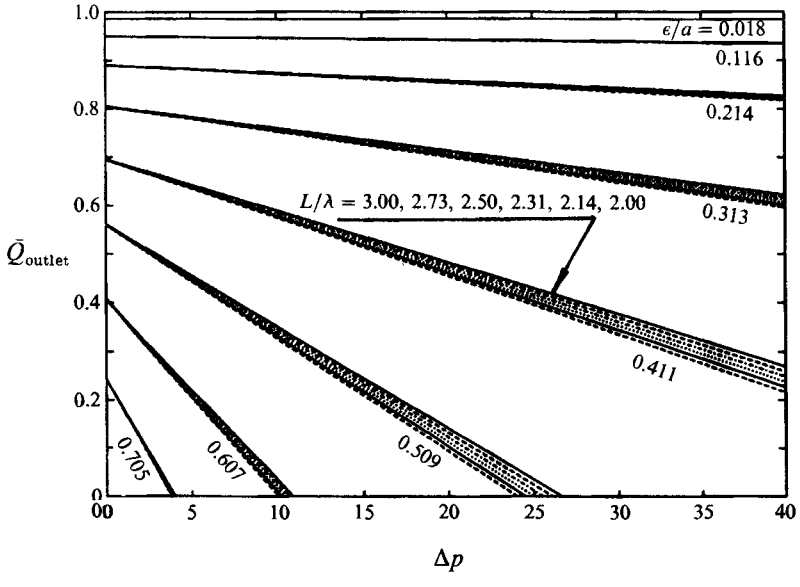

FIGURE 13. Pressure–volume flow rate characteristics of single wave peristaltic transport with different relative tube occlusions ϵ/a and different tube-to-wave lengths L/λ. The average volume flow rate at the tube outlet $\bar{Q}_{\text{outlet}}$ is plotted against pressure difference $\Delta p = p_L - p_0$ in groups for different ϵ/a, where L/λ is varied within each group from 3 to 2 in the direction indicated by the arrow.

increases with increasing L/λ; this is not the case in the train-wave peristaltic transport.

5. Discussion and conclusions

Previous studies of peristaltic transport have universally considered periodic peristaltic waves in infinite tubes, ignoring the inherently non-steady effects associated with the finite-length tubes encountered in real peristaltic pumps and in physiological peristaltic flows. Physiologically, transport by a single bolus moving along a tube of finite length is of particular interest, as occurs in the oesophagus for example. In the oesophagus, intraluminal pressure data for clinical evaluation are collected at select points along the length of the lumen, sometimes concurrent with radiographic imaging. An issue of great physiological concern is the interpretation of the spatial–temporal variations in local stresses in terms of the motility and efficacy of the transport process (Brasseur & Dodds 1991). Past studies of peristaltic transport have concentrated, to a large extent, on global pumping characteristics of peristaltic pumps. In this study we focus on both local and global dynamics.

Using the lubrication-theory approximations, we have studied in detail the sources of non-steadiness in the internal fluid stresses induced by the finite length of the peristaltic pump, the effects of non-integral numbers of peristaltic waves within a tube with fixed pressure at its ends, particle motion and fluid transport with single peristaltic waves, and global pumping performance. Unlike the infinite-tube model, fixed pressure at the tube ends induces large global fluctuations in pressure as the peristaltic waves pass through the tube inlet or outlet. In addition to these global fluctuations, fluctuations in pressure arise also from the existence of non-integral numbers of peristaltic waves within the tube. These additional fluctuations arise from a phase mismatch between peristaltic waves entering the tube and waves leaving the tube.

Similar statements may be made concerning shear stress variations within the peristaltic pump. Peristalsis produces very large shear stress, and very large gradients in shear stress in the zone of maximal occlusion. Indeed, the creation of large shear forces in the contraction zone is the dominant mechanism behind peristaltic transport. We have found that peak shear stress fluctuates with time, and attains larger values with non-integral numbers of peristaltic waves. Global pumping performance, on the other hand, is only slightly degraded by the existence of non-integral numbers of peristaltic waves in a finite-length tube.

Of particular physiological interest are the characteristics of single-wave bolus transport, in comparison with train-wave peristaltic transport. A train of peristaltic waves, on average, transports fluid in the direction of peristalsis in the same way at all cross-sections within the tube. This is not the case with single-wave transport. In fact, retrograde fluid motion occurs everywhere within the tube except within the peristaltic wave itself. Consequently, fluid continuously leaves the tube inlet during single-wave bolus transport. Similarly, fluid continuously enters the tube at the tube outlet at all times except as the peristaltic wave leaves the tube carrying bolus fluid with it. When averaged over the transit time of the single wave, however, the net effect is transport of fluid from the tube outlet.

Owing to strong retrograde motion proximal to the peristaltic wave, single-wave peristaltic transport is associated with much higher levels of fluid particle reflux than train-wave transport. We further show that the degree of fluid particle reflux is a

strong function of the shape of the peristaltic wave, but only slightly affected by the existence of non-integral numbers of train waves within the peristaltic pump.

Pumping by a train of peristaltic waves requires the existence of an adverse pressure difference across the tube ends to create particle reflux. By contrast, single-wave pumps require a favourable pressure difference to prevent particle reflux through the tube inlet. Furthermore, when the single-wave pump is operating at given fixed pressure difference between the pump ends, a 'critical' tube occlusion exists at which retrograde flow of fluid from the inlet is maximal. Occlusions larger or smaller than this critical value reduce the average rate of flow from the tube inlet. Similar to train-wave pumps, pumping performance with single-wave transport is not strongly affected by different L/λ. On the other hand, train waves will be more effective at continuous fluid pumping than widely spaced single peristaltic waves.

In summary, whereas global pumping performance is altered to a relatively minor extent when the finite length of the peristaltic pump is taken into account, local effects – temporal and spatial variations in pressure and shear stress, retrograde flow, and particle motions within the bolus fluid – are strongly affected by the finite extent of the tube, the existence of integral *vs.* non-integral numbers of peristaltic waves within the tube, and the shape of the peristaltic wave. These local effects are of importance in the interpretation of manometric measurements of intraluminal pressure in physiological peristaltic flows, and should be taken into account in the design of commercial peristaltic pumps.

We wish to acknowledge with fondness our continued interactions on the issues of peristalsis in the human swallowing process with Wylie Dodds, M.D., Benson Massey, M.D., Mark Kern, M.S., and Walt Hogan, M.D. at the Medical College of Wisconson, and Martin Donner, M.D., Bronwyn Jones, M.D., and William Ravich, M.D. at the Johns Hopkins Medical Institutions. We especially acknowledge our good friends Wylie Dodds and Martin Donner, who recently passed away. This research was carried out under NIH grant RO1-DK41436; this support is gratefully acknowledged.

REFERENCES

Barton, C. & Raynor, S. 1968 Peristaltic flow in tubes. *Bull. Math. Biophys.* **30**, 663–680.

Bohme, G. B. & Friedrich, R. 1983 Peristaltic flow of viscoelastic liquids. *J. Fluid Mech.* **128**, 109–122.

Brasseur, J. G., Corrsin, S. & Lu, N. Q. 1987 The influence of a peripheral layer of different viscosity on peristaltic pumping with Newtonian fluid. *J. Fluid Mech.* **174**, 495–519.

Brasseur, J. G. & Dodds, W. J. 1991 Interpretation of intraluminal manometric measurements in terms of swallowing mechanics. *Dysphagia* **6**, 100–119.

Brown, T. D. & Hung, T.-K. 1977 Computational and experimental investigations of two-dimensional nonlinear peristaltic flows. *J. Fluid Mech.* **83**, 249–272.

Burns, J. C. & Parkes, T. 1967 Peristaltic motion. *J. Fluid Mech.* **29**, 731–743.

Dusey, M. P., Brasseur, J. G. & Li, M.-J. 1990 Analysis of a singularity inherent to the lubrication theory model of peristaltic pumping using a full Navier–Stokes simulation (abstract). *Bull. Am. Phys. Soc.* **35**, 2245.

Fung, Y. C. & Yih, C. S. 1968 Peristaltic transport. *Trans. ASME* E: *J. Appl. Mech.* **35**, 669–675.

Hanin, M. 1968 The flow through a channel due to transversely oscillating walls. *Israel J. Tech.* **6**, 67–71.

Jaffrin, M. Y. 1973 Inertia and streamline curvature on peristaltic pumping. *Intl. J. Engng. Sci.* **11**, 681–699.

Jaffrin, M. Y. & Meginniss, J. R. 1971 The hydrodynamics of roller pumps and their

implication to hemolysis. *Fluid Mechanics Laboratory, Publication No.* 71-1. Department of Mechanical Engineering, Massachusetts Institute of Technology, Cambridge, MA.

JAFFRIN, M. Y. & SHAPIRO, A. H. 1971 Peristaltic pumping. *Ann. Rev. Fluid Mech.* **3**, 13–36.

LATHAM, T. W. 1966 Fluid motions in a peristaltic pump. M.S. thesis, Massachusetts Institute of Technology, Cambridge, MA.

LIU, N. S. & KRAUSE, E. 1979 Calculation of incompressible viscous flows in vessels with moving boundaries. *Acta Mechanica* **33**, 21–32.

LYKOUDIS, P. S. & ROOS, R. 1970 The fluid mechanics of the ureter from a lubrication theory point of view. *J. Fluid Mech.* **43**, 661–674.

RATH, H. J. 1982 Peristaltic flow through a lobe-shaped tube. *Intl. J. Mech. Sci.* **24**, 359–367.

ROOS, R. & LYKOUDIS, P. S. 1971 The fluid mechanics of the ureter with an inserted catheter. *J. Fluid Mech.* **46**, 625–630.

SHAPIRO, A. H. 1967 Pumping and retrograde diffusion in peristaltic waves. *Proc. Workshop on Ureteral Reflux in Children.* Natl. Acad. Sci. Washington, D.C.

SHAPIRO, A. H., JAFFRIN, M. Y. & WEINBERG, S. L. 1969 Peristaltic pumping with long wavelengths at low Reynolds number. *J. Fluid Mech.* **37**, 799–825.

SHUKLA, J. B. & GUPTA, S. P. 1982 Peristaltic transport of a power-law fluid with variable consistency. *Trans. ASME* K: *J. Biomech Engng* **104**, 182–186.

SHUKLA, J. B., PARIHAR, R. S., RAO, B. R. P. & GUPTA, S. P. 1980 Effects of peripheral-layer viscosity on peristaltic transport of a bio-fluid. *J. Fluid mech.* **97**, 225–237.

STAVITSKY, D., MACAGNO, E. O. & CHRISTENSEN, J. 1981 Finite-element analysis of flow induced by contractions like those of intestine. *J. Biomech.* **14**, 183–193.

TAKABATAKE, S. & AYUKAWA, K. 1982 Numerical study of two-dimensional peristaltic flows. *J. Fluid Mech.* **122**, 439–465.

TAKABATAKE, S., AYUKAWA, K. & MORI, A. 1988 Peristaltic pumping in circular cylindrical tubes: a numerical study of fluid transport and its efficiency. *J. Fluid Mech.* **193**, 267–283.

TAYLOR, G. I. 1951 analysis of the swimming of microscopic organisms. *Proc. R. Soc. Lond.* A**209**, 447–461.

TONG, P. & VAWTER, D. 1972 An analysis of peristaltic pumping. *Trans. ASME* E: *J. Appl. Mech.* **39**, 857–862.

WEINBERG, S. L., ECKSTEIN, E. C. & SHAPIRO, A. H. 1971 An experimental study of peristaltic pumping. *J. Fluid Mech.* **49**, 461–497.

YIH, F. & FUNG, Y. C 1969 Peristaltic waves in circular cylindrical tubes. *Trans. ASME* E: *J. Appl. Mech.* **36**, 579–587.